Phase behavior of liquid-crystal monolayers of rod-like and plate-like particles

Yuri Martínez-Ratón

*Grupo Interdisciplinar de Sistemas Complejos (GISC), Departamento de Matemáticas, Escuela Politécnica Superior, Universidad Carlos III de Madrid, Avenida de la Universidad 30, E-28911, Leganés, Madrid, Spain**

Szabolcs Varga

Institute of Physics and Mechatronics, University of Pannonia, PO Box 158, Veszprém, H-8201 Hungary†

Enrique Velasco

Departamento de Física Teórica de la Materia Condensada, Instituto de Ciencia de Materiales Nicolás Cabrera and Condensed Matter Physics Center (IFIMAC), Universidad Autónoma de Madrid, E-28049 Madrid, Spain‡

arXiv:1403.3372v1 [cond-mat.soft] 13 Mar 2014

Abstract

Orientational and positional ordering properties of liquid crystal monolayers are examined by means of Fundamental-Measure Density Functional Theory. Particles forming the monolayer are modeled as hard parallelepipeds of square section of size σ and length L. Their shapes are controlled by the aspect ratio $\kappa = L/\sigma$ (> 1 for prolate and < 1 for oblate shapes). The particle centers of mass are restricted to a flat surface and three possible and mutually perpendicular orientations (in-plane and along the layer normal) of their uniaxial axes are allowed. We find that the structure of the monolayer depends strongly on particle shape and density. In the case of rod-like shapes, particles align along the layer normal in order to achieve the lowest possible occupied area per particle. This phase is a uniaxial nematic even at very low densities. In contrast, for plate-like particles, the lowest occupied area can be achieved by random in-plane ordering in the monolayer, i.e. planar nematic ordering takes place even at vanishing densities. It is found that the random in-plane ordering is not favorable at higher densities and the system undergoes an in-plane ordering transition forming a biaxial nematic phase or crystallizes. For certain values of the aspect ratio, the uniaxial-biaxial nematic phase transition is observed for both rod-like and plate-like shapes. The stability region of the biaxial nematic phase enhances with decreasing aspect ratios for plate-like particles, while the rod-like particles exhibit a reentrant phenomenon, i.e. a sequence of uniaxial-biaxial-uniaxial nematic ordering with increasing density if the aspect ratio is larger than 21.34. In addition to this, packing fraction inversion is observed with increasing surface pressure due to the alignment along the layers normal. At very high densities the nematic phase destabilizes to a nonuniform phases (columnar, smectic or crystalline phases) for both shapes.

PACS numbers: 61.30.Pq,64.70.M-,47.57.J-

*Electronic address: yuri@math.uc3m.es

†Electronic address: vargasz@almos.uni-pannon.hu

‡Electronic address: enrique.velasco@uam.es

I. INTRODUCTION

Understanding the ordering properties of liquid crystals in restricted geometry is still a challenging problem [1]. It is well known that the confinement of rod-like or plate-like particles into two dimensions has great impact on the phase behaviour of the system. For example, the isotropic-nematic phase transition of three-dimensional (3D) hard ellipsoids is of first order [2], but when the centers of mass and orientations of the long axis of the particles are restricted to be on a plane, which corresponds to a two-dimensional (2D) system of hard ellipses, a continuous isotropic-nematic phase transition can be observed (via a Kosterlitz-Thouless disclination unbinding type mechanism with a nematic phase exhibiting only quasi-long-range orientational order [3]). The defect structure of a 2D nematic phase is also nontrivial [4–6]. In addition to this, the dynamics of 2D hard ellipses shows peculiarities in the rotational and translational diffusions and in the glassy behaviours [7, 8]. Recently, a two-step glass transition has been observed in a monolayer of colloidal ellipsoids confined between two glass walls. In the first step, an orientational glass emerges with increasing density, which is related to orientational arrest of the particles, while in the second the system becomes translationally frozen at higher densities [9, 10]. The structural and dynamical properties of 2D and even 1D complex fluids have recently become experimentally accessible due to the development of nanofluidics and optical trapping methods. Liquid-crystal monolayers can be prepared by confining colloidal particles between parallel walls [11, 12] or by spreading colloidal nanoparticles or amphiphilic molecules at the air/liquid interface [13, 14]. This makes it possible to study the competition between the orientational and packing entropies in restricted geometries [12]. Even the ordering effect of surface patchiness has been examined in a monolayer of nanoplatelets [15].

The difference between the phase behaviours of molecularly thick films (Langmuir monolayers) and that of colloidal monolayers confined between two parallel planes is mainly due to the fact that the amphiphilic molecules are allowed to rotate out from the air/liquid interface, while the colloids can rotate only in the plane parallel to the confining walls. The consequence is that the phase behaviour of Langmuir monolayers can be much richer than that of 2D colloidal systems. For example, upon compression, only a few phases (isotropic, nematic, solid) may occur if the confined particles have only 2D orientational freedom [6, 17], while several additional, tilted or not tilted, phases can be present in the case of Langmuir

monolayers with out-of-plane rotational freedom [18–20] due to their intermediate quasi-two-dimensional character (i.e. 2D in translations and 3D in orientations). Therefore it is worth studying the effect of the orientational freedom and its coupling with the translational part on the ordering properties of simple model systems. A model of confined hard particles is ideal, since it is amenable to theoretical analysis and, as is well known from numerous studies on liquid-crystalline ordering, can give rise to nontrivial behaviour.

In our study we examine the phase behaviour of uniaxial hard parallelepipeds confined such that their centers of mass are forced to be on a plane, while they are allowed to rotate out of the plane. Our aim is to determine the effect of the additional, out-of-plane, orientational freedom on the stability of the isotropic, nematic and solid phases of 2D hard rectangles. Depending on the aspect ratio of the parallelepipeds, it is possible to study the phase behaviour of both rod-like (prolate shaped) and plate-like (oblate shaped) particles. In the case of rod-like particles, steric (excluded volume) interactions favour orientational ordering along the layer normal even at low densities, because out-of-plane ordering produces low surface coverage. However, the situation is very different in the case of oblate shapes, because when particles lie on the plane the occupied area on the surface is increased. Therefore, steric interactions act on the plate-like particles so as to promote rotation out of the confining plane. In such situation biaxial nematic ordering may emerge in the monolayer, because both symmetry axes of the particles can be ordered at high surface coverage. We pay special attention to the determination of the stability region of biaxial nematic phase for both shapes. Note that the biaxial nematic phase has been only stabilized in systems of biaxial hard particles [21–24], while our model system is uniaxial and the confinement gives rise to biaxial ordering.

The article is arranged as follows: Sec. II is devoted to presenting the model for the monolayer and the density-functional theory (DFT) and related tools used to calculate phase diagrams; in Sec. II A we focus on the nematic phases, while in Sec. II B we present details on the bifurcation analysis used to calculate the spinodal instabilities of the nematic phase with respect to nonuniform phases. The results are shown in Sec. III for prolate (Sec. III A) and oblate (Sec. III B) particle geometries. Some conclusions are drawn in Sec. IV.

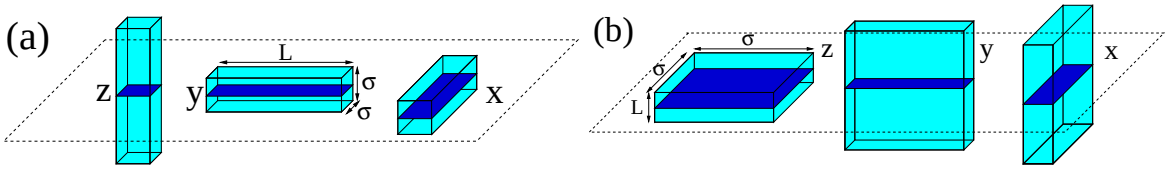

FIG. 1: Possible orientations of confined (a) prolate and (b) oblate uniaxial parallelepipeds in the Zwanzig approximation. The projection of the original particles onto a plane are shown in dark. Different species are correspondingly labelled and their characteristic lengths are also shown.

II. ZWANZIG MODEL FOR 3D HARD RODS PROJECTED ON A PLANE

We use a Zwanzig approximation, where particles are restricted to orient along x, y and z axes only. The model is defined by three parallelepipedic species of length L and square cross-sectional area σ^2 (σ being the particle breadth). The aspect ratio $\kappa = L/\sigma$ can be larger (prolate geometry) or smaller (oblate geometry) than unity. The three species are labelled as x, y and z, meaning that the longest (prolate shape) and shortest (oblate shape) axis of the particles is parallel to the x, y or z Cartesian axes. The particle centers of mass are restricted to lie on a plane perpendicular to z and located at $z = 0$. Therefore, the 3D density profiles are

$$\rho_\nu^{(3D)}(x, y, z) = \rho_\nu^{(2D)}(x, y)\delta(z), \quad \nu = x, y, z, \tag{1}$$

with $\delta(z)$ the Dirac-delta function. $\rho_\nu^{(2D)}(x, y)$ is the 2D density profile of species ν on the plane. There are three possible projections of the particles on the plane (Fig. 1): two rectangles, with their distinct axis parallel to x or y, of width σ and length L, and a square of side-length σ. Thus our model becomes effectively a 2D ternary mixture of two species of mutually perpendicular hard rectangles and a third species consisting of hard squares.

The DFT theory for the 2D ternary mixture model defined above can be obtained from the Fundamental-Measure DFT expression for a system of 3D hard parallelepipeds in the Zwanzig approximation, as we now show. The excess part of the latter has the form

$$\mathcal{F}_{\rm ex}^{(3D)}[\{\rho_\nu^{(3D)}\}] = \int dx \int dy \int dz\ \Phi_{3D}(x, y, z), \tag{2}$$

where $\Phi_{3D}(x, y, z)$ is the excess part of the free-energy density (see [25] for details). This functional fulfills the dimensional crossover property: when the constrained density profiles

(1) are inserted into (2), one obtains the free-energy functional of the 2D projected fluid:

$$\mathcal{F}_{\rm ex}^{(3D)}[\{\rho_\nu^{(3D)}\}] \to \mathcal{F}_{\rm ex}^{(2D)}[\{\rho_\nu^{(2D)}\}] = \int dx \int dy\ \Phi_{2D}(x,y), \tag{3}$$

with $\Phi_{2D}(x,y)$ the excess part of the free-energy density of the 2D ternary mixture [25]:

$$\Phi_{2D}(\boldsymbol{r}) = -n_0(\boldsymbol{r})\ln[1-n_2(\boldsymbol{r})] + \frac{n_{1x}(\boldsymbol{r})n_{1y}(\boldsymbol{r})}{1-n_2(\boldsymbol{r})}, \tag{4}$$

where the notation $\boldsymbol{r} \equiv (x,y)$ has been used. The weighted densities are given by

$$n_\alpha(\boldsymbol{r}) = \sum_{\nu=\{x,y,z\}} \int d\boldsymbol{r}' \rho_\nu^{(2D)}(\boldsymbol{r}')\omega_\nu^{(\alpha)}(\boldsymbol{r}-\boldsymbol{r}') \tag{5}$$

with

$$\begin{aligned}
\omega_\nu^{(0)}(\boldsymbol{r}) &= \frac{1}{4}\delta\left(\frac{\sigma_\nu^x}{2}-|x|\right)\delta\left(\frac{\sigma_\nu^y}{2}-|y|\right), \\
\omega_\nu^{(1x)}(\boldsymbol{r}) &= \frac{1}{2}\Theta\left(\frac{\sigma_\nu^x}{2}-|x|\right)\delta\left(\frac{\sigma_\nu^y}{2}-|y|\right), \\
\omega_\nu^{(1y)}(\boldsymbol{r}) &= \frac{1}{2}\delta\left(\frac{\sigma_\nu^x}{2}-|x|\right)\Theta\left(\frac{\sigma_\nu^y}{2}-|y|\right), \\
\omega_\nu^{(2)}(\boldsymbol{r}) &= \Theta\left(\frac{\sigma_\nu^x}{2}-|x|\right)\Theta\left(\frac{\sigma_\nu^y}{2}-|y|\right),
\end{aligned} \tag{6}$$

$\Theta(x)$ is the Heaviside function and we have defined $\sigma_\nu^\mu \equiv \sigma + (L-\sigma)\delta_{\mu\nu}$, with $\delta_{\mu\nu}$ the Kronecker delta. Note that $\mu = \{x,y\}$ while $\nu = \{x,y,z\}$. The ideal part of the free-energy is

$$\beta\mathcal{F}_{\rm id}[\{\rho_\mu\}] = \sum_{\nu=\{x,y,z\}} \int d\boldsymbol{r}\rho_\nu^{(2D)}(\boldsymbol{r})\left[\ln\rho_\nu^{(2D)}(\boldsymbol{r})-1\right]. \tag{7}$$

Note that we have dropped the thermal volume Λ^3 inside the logarithm of Eq. (7) as it does not affect the phase behaviour of the system.

A. The nematic phase

For uniform density profiles we have $\rho_\nu^{(2D)} = \gamma_\nu\rho_{2D}$, with $\rho_{2D} = N/A$ the total surface density and γ_ν the molar fraction of species ν, which satisfies the constraint $\sum_\nu \gamma_\nu = 1$. For a general biaxial nematic phase, $\mathrm{N_b}$, we parameterize γ_ν as

$$\gamma_x = \frac{1-Q_{\rm u}}{3} + \frac{Q_{\rm b}}{2}, \quad \gamma_y = \frac{1-Q_{\rm u}}{3} - \frac{Q_{\rm b}}{2}, \quad \gamma_z = \frac{1+2Q_{\rm u}}{3}, \tag{8}$$

where $Q_{\rm u} \in [-1/2, 1]$ is the usual uniaxial nematic order parameter and $Q_{\rm b} \equiv \gamma_x - \gamma_y$ measures the biaxiality in the $x-y$ plane. The uniaxial nematic phase N_u has $Q_{\rm b} = 0$. In terms of the order parameters, the ideal and excess parts of the free-energy density in reduced units become

$$\frac{\beta \mathcal{F}_{\rm id} a}{V} = \rho^* \left[\ln \rho^* - 1 + \sum_{\nu=x,y,z} \gamma_\nu \left(Q_{\rm u}, Q_{\rm b}\right) \ln \gamma_\nu \left(Q_{\rm u}, Q_{\rm b}\right) \right],$$

$$\frac{\beta \mathcal{F}_{\rm ex} a}{V} = -\rho^* \ln \left[1 - \eta(Q_{\rm u})\right] + \frac{\kappa \left(\rho^*\right)^2}{1 - \eta(Q_{\rm u})} \left[\frac{1}{9} \left(1 + \frac{2}{\kappa} - \left(1 - \frac{1}{\kappa}\right) Q_{\rm u} \right)^2 - \frac{1}{4} \left(1 - \frac{1}{\kappa}\right)^2 Q_{\rm b}^2 \right], \quad (9)$$

with V the total volume of the system, and $\rho^* = \rho_{\rm 2D} a$ (with $a = L\sigma$ the area of the rectangular species x and y) a scaled 2D density and $\kappa = L/\sigma$ the aspect ratio. The uniform limit of the weighted density $n_2(\boldsymbol{r})$ is the packing fraction $\eta = \dfrac{N}{A} \sum_\nu \gamma_\nu a_\nu$ (with $a_x = a_y = L\sigma$ and $a_z = \sigma^2$), which depends on $Q_{\rm u}$:

$$\eta(Q_{\rm u}) = \frac{\rho^*}{3} \left[2 + \frac{1}{\kappa} - 2 \left(1 - \frac{1}{\kappa}\right) Q_{\rm u} \right]. \quad (10)$$

Minimization of the total free energy $\beta \mathcal{F} a/V = \beta \left(\mathcal{F}_{\rm id} + \mathcal{F}_{\rm ex}\right) a/V$ with respect to the order parameters $Q_{\rm u}$ and $Q_{\rm b}$ gives a pair of nonlinear equations that have to be solved iteratively:

$$Q_{\rm u} = \frac{1 - e^{-H_1(Q_{\rm u}, Q_{\rm b})} \cosh\left[H_2(Q_{\rm u}, Q_{\rm b})\right]}{1 + 2e^{-H_1(Q_{\rm u}, Q_{\rm b})} \cosh\left[H_2(Q_{\rm u}, Q_{\rm b})\right]},$$

$$Q_{\rm b} = \frac{2e^{-H_1(Q_{\rm u}, Q_{\rm b})} \sinh\left[H_2(Q_{\rm u}, Q_{\rm b})\right]}{1 + 2e^{-H_1(Q_{\rm u}, Q_{\rm b})} \cosh\left[H_2(Q_{\rm u}, Q_{\rm b})\right]}, \quad (11)$$

where we have defined

$$H_1(Q_{\rm u}, Q_{\rm b}) = \frac{\rho^*}{1 - \eta(Q_{\rm u})} \left(1 - \frac{1}{\kappa}\right) \left\{ 1 + \frac{\kappa}{3} \left(1 + \frac{2}{\kappa} - \left(1 - \frac{1}{\kappa}\right) Q_{\rm u} \right) + \frac{\kappa \rho^*}{1 - \eta(Q_{\rm u})} \left[\frac{1}{9} \left(1 + \frac{2}{\kappa} - \left(1 - \frac{1}{\kappa}\right) Q_{\rm u} \right)^2 - \frac{1}{4} \left(1 - \frac{1}{\kappa}\right)^2 Q_{\rm b}^2 \right] \right\},$$

$$H_2(Q_{\rm u}, Q_{\rm b}) = \frac{\kappa \rho^*}{2[1 - \eta(Q_{\rm u})]} \left(1 - \frac{1}{\kappa}\right)^2 Q_{\rm b}. \quad (12)$$

The N_u-N_b bifurcation can be calculated by solving Eqns. (11), expanded up to first order with respect to $Q_{\rm b}$. After some algebra, we arrive at the non-linear equation

$$f(y, \kappa) \equiv y(\kappa^2 - 1) - 2 - \exp\left\{ \kappa \left[\frac{\left(y(1 + \kappa^{-1}) + 1\right)^2}{1 - \kappa^{-1}} - 1 \right] \right\} = 0. \quad (13)$$

for the variable $y \equiv \rho_{2D}\sigma^2/(1-\rho_{2D}\sigma^2)$ [note that $\rho^* = y\kappa/(1+y)$]. One obtains a continuous N_u-N_b phase transition, with a phase boundary in the density–aspect ratio plane given by a curve $y(\kappa)$ or $\rho^*(\kappa)$; the uniaxial order parameter Q_u and the packing fraction η at bifurcation can be calculated as a function of y as

$$Q_u = 1 - \frac{3}{y(\kappa^2-1)}, \qquad \eta = (1+y)^{-1}\left(y + \frac{2}{\kappa+1}\right). \tag{14}$$

The asymptotic limit $\kappa \to 0$ (infinitely thin plates) of Eq. (13) is $|y| - 2 = e^{-y^2}$, the solution y_a of which gives $\eta_a = (|y_a| - 2)/(|y_a| - 1) = 0.01681$. The other asymptotic limit of (13) for prolate particles, $\kappa \to \infty$ (needles), will be discussed later.

The critical end-point (y_0, κ_0) of the transition curve N_u-N_b, if it exists, can be found from the solution of the equations

$$f(y_0, \kappa_0) = \frac{\partial f}{\partial y}(y_0, \kappa_0) = 0, \tag{15}$$

which results in the following trascendental equation:

$$\frac{1}{4y_0(1+y_0)^2} = \exp\left\{\frac{(1+2y_0)(3+2y_0)[2+(3+2y_0)y_0]}{2(1+y_0)} - 1\right\}, \quad \kappa_0 = 1 + \frac{1+2y_0}{2y_0(1+y_0)}. \tag{16}$$

Solving for prolate parallelepipeds ($\kappa > 1$), we obtain the solutions $\rho_0^* = 0.52427$ and $\kappa_0 = 21.33910$. No solution has been found for oblate parallelepipeds.

B. The nematic to non-uniform phases instabilities

The Fourier transforms of the direct correlation functions can be written as

$$-\hat{c}_{\mu\nu}(\boldsymbol{q}, \rho^*, \{Q_\alpha\}) = \sum_{\alpha,\beta} \frac{\partial^2 \Phi_{2D}(\rho^*, \{Q_\alpha\})}{\partial n_\alpha \partial n_\beta} \hat{\omega}_\mu^{(\alpha)}(\boldsymbol{q}) \hat{\omega}_\nu^{(\beta)}(\boldsymbol{q}), \tag{17}$$

where $\boldsymbol{q} = (q_x, q_y)$ is the wave vector. The Fourier transforms of the weighting functions are given by

$$\hat{\omega}_\nu^{(0)}(\boldsymbol{q}) = \chi_0\left(q_x\frac{\sigma_\nu^x}{2}\right)\chi_0\left(q_y\frac{\sigma_\nu^x}{2}\right), \quad \hat{\omega}_\nu^{(1x)}(\boldsymbol{q}) = \sigma_\nu^x\chi_1\left(q_x\frac{\sigma_\nu^x}{2}\right)\chi_0\left(q_y\frac{\sigma_\nu^y}{2}\right),$$

$$\hat{\omega}_\nu^{(1y)}(\boldsymbol{q}) = \sigma_\nu^y\chi_0\left(q_x\frac{\sigma_\nu^x}{2}\right)\chi_1\left(q_y\frac{\sigma_\nu^y}{2}\right), \quad \hat{\omega}_\nu^{(2)}(\boldsymbol{q}) = \sigma_\nu^x\sigma_\nu^y\chi_1\left(q_x\frac{\sigma_\nu^x}{2}\right)\chi_1\left(q_y\frac{\sigma_\nu^y}{2}\right), \tag{18}$$

with $\chi_0(x) = \cos x$ and $\chi_1(x) = \sin(x)/x$. The instabilities of the nematic phase against spatially-nonuniform fluctuations can be found from the equations

$$T(\boldsymbol{q}, \rho^*, \{Q_\alpha\}) = 0, \quad \boldsymbol{\nabla}_{\boldsymbol{q}} T(\boldsymbol{q}, \rho^*, \{Q_\alpha\}) = 0, \tag{19}$$

where

$$T(\boldsymbol{q}, \rho^*, \{Q_\alpha\}) = \det \left[\frac{\delta_{\mu\nu}}{\rho_\mu} - \hat{c}_{\mu\nu}(\boldsymbol{q}, \rho^*, \{Q_\alpha\}) \right], \quad \mu, \nu = x, y, z, \tag{20}$$

and 'det' denotes a determinant. Thus we obtain the values of ρ_0^* and $\boldsymbol{q}_0$ at bifurcation, and the order parameters $\{Q_\alpha\}$ come from Eqns. (11). In practical terms we proceed by fixing the direction of the wavevector as follows: (i) $\boldsymbol{q} = (0, q)$, which implies columnar (C) symmetry if $Q_\mathrm{b} > 0$ or plastic (K) symmetry if $Q_\mathrm{b} = 0$; (ii) $\boldsymbol{q} = (q, 0)$, which implies smectic (S) symmetry if $Q_\mathrm{b} > 0$. The C phase is defined as a 2D layered phase in which the 2D nematic director is parallel to the layers (or columns) while in the S phase the director is perpendicular to the layers. The value of q can be obtained by solving Eqns. (19).

III. RESULTS

In this section we present the results for the model as obtained from (i) minimization of the free-energy density and (ii) bifurcation analysis of the continuous $\mathrm{N_u}$-$\mathrm{N_b}$ transitions for rods and plates or the spinodal instabilities from uniform to nonuniform phases. The phase behaviour of prolate and oblate particles are explained in different sections.

A. Prolate particles

Fig. 2(a) contains the results obtained from the solutions of Eqns. (11) for the equilibrium order parameters Q_u and Q_b as a function of ρ^* for particles with aspect ratios $1 < \kappa \leq 20$. In this range of κ we always find that $Q_b = 0$, i.e. the $\mathrm{N_u}$ is the only stable phase. As can be seen from the figure, the uniaxial order parameter Q_u increases from zero and saturates with ρ^*. The system does not exhibit any orientational ordering phase transition (at zero density the order parameter departs from zero with a finite derivative). The order of rods builds up continuously with density along the direction perpendicular to the monolayer. The $\mathrm{N_u}$ phase is depicted in Fig. 3(a), where the cross sections of particles are sketched: the most

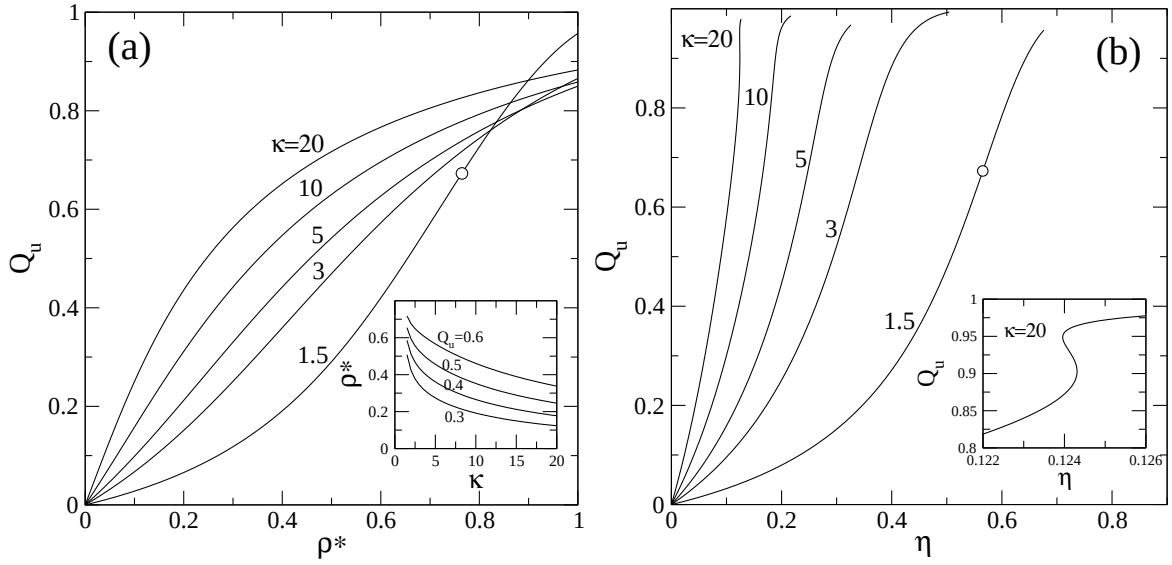

FIG. 2: (a) Uniaxial parameter $Q_{\rm u}$ as a function of the scaled density ρ^* for different values of κ (labelled in the figure). Inset: ρ^* as a function of κ for various values of $Q_{\rm u}$ (correspondingly labelled). (b) $Q_{\rm u}$ as a function of packing fraction η. Inset: detail of the curve corresponding to $\kappa = 20$. The empty circle in both panels represents the location of the N_u-C,K bifurcation as calculated from the bifurcation analysis.

populated species corresponds to squares, while the probabilities to find rectangular species pointing along x or y are equal.

The inset of Fig. 2(a) shows that ρ^* is a monotonically decreasing function of κ for fixed value $0.3 \leq Q_{\rm u} \leq 0.6$. As rods become longer, a fixed amount of nematic order requires a lower density. For higher values of $Q_{\rm u}$ this is not true (see main figure); however, when using $\rho_{\rm 2D}\sigma^2$ (mean particle number in a fraction σ^2/A of the total area A) instead of ρ^* as a density variable the trend is restored, since the ratio $\rho_{\rm 2D}\sigma^2/\rho^* = \kappa^{-1}$ decreases strongly with κ. Finally the empty circle in Fig. 2 represent the location of the N_u-C,K bifurcation as calculated from the bifurcation analysis. We will return to this point later.

In Fig. 2(b) we plot $Q_{\rm u}$ as a function of the packing fraction η. Now the curves do not intersect each other for any κ, but for large κ (~ 20) they exhibit a loop (see inset). The loop is not a signature of any phase transition, and is simply related with the dependence of η with the order parameter $Q_{\rm u}$, as is explained in the following. From Eqn. (10) we can approximate $\eta(Q_{\rm u}) \approx \dfrac{2\rho^*}{3}(1 - Q_{\rm u})$ when $\kappa^{-1} \ll 1 - Q_{\rm u}$. If $Q_{\rm u} \sim 1$, taking into account that $Q_{\rm u}$ is a monotonically increasing function of ρ^*, the lowering of $1 - Q_{\rm u}$ can compensate,

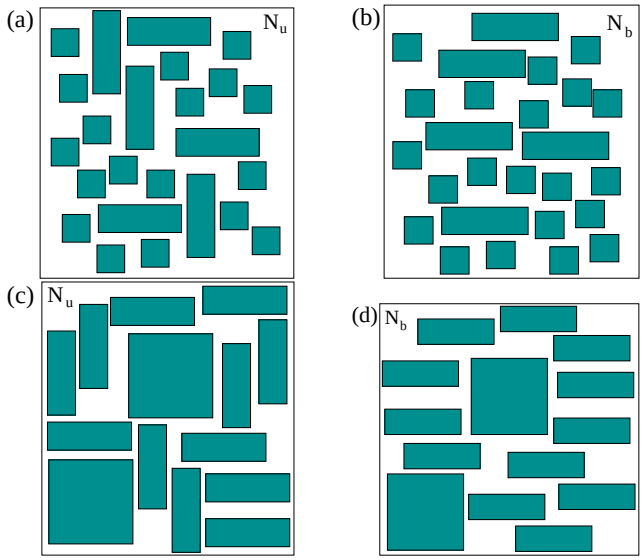

FIG. 3: Sketch of cross-sectional particle configurations in the N_u phase [(a) for prolate and (c) for oblate particles] and N_b phase [(b) for prolate and (c) for oblate particles].

for certain values of ρ^*, the increment of the latter, giving a decrease in η. Further, when $\kappa^{-1} \gg 1 - Q_u$, we have $\eta(Q_u) \approx \dfrac{\rho^*}{3\kappa}(1 + 2Q_u)$, an increasing function of ρ^*.

When the aspect ratio κ is high enough (for $\kappa > \kappa_0 \simeq 21.339$) two solutions of Eqn. (13) exist, associated with two N_u-N_b bifurcation points. Therefore, the sequence N_u-N_b-N_u is obtained as a function of density. To analyse this in more detail, the free energies of the N_u and N_b phases as a function of ρ^* were calculated. The results are plotted in Fig. 4(a) for $\kappa = 40$. Both N_u-N_b transitions are continuous. The inset shows the order parameters Q_u and Q_b as a function of ρ^*. The mean-field behaviour $Q_b \sim |\rho^* - \rho_b^*|^{1/2}$ as $\rho^* \to \rho_b^*$ is confirmed, where ρ_b^* corresponds to any of the two bifurcation values. In Fig. 3(b) the particle cross sections for the N_b phase are sketched in a situation where the majority of rectangular species point to the x axis, $Q_b \sim \gamma_x$ (i.e. the biaxial parameter is almost saturated; note that it can only saturate in a system of plates).

We can explain the presence of the reentrant N_b phase as follows. The strictly 2D fluid composed of hard-rectangular particles exhibits a continuous I-N_u transition at a packing fraction that decreases with aspect ratio as $\eta_{2D} = 2/(\kappa + \kappa^{-1})$ (in the Zwanzig approximation). For the 3D Zwanzig rod fluid with centers of mass constrained on a plane, the packing fractions of parallelepipeds with rectangular projection, $\eta_{xy} \equiv \eta_x + \eta_y$, and square

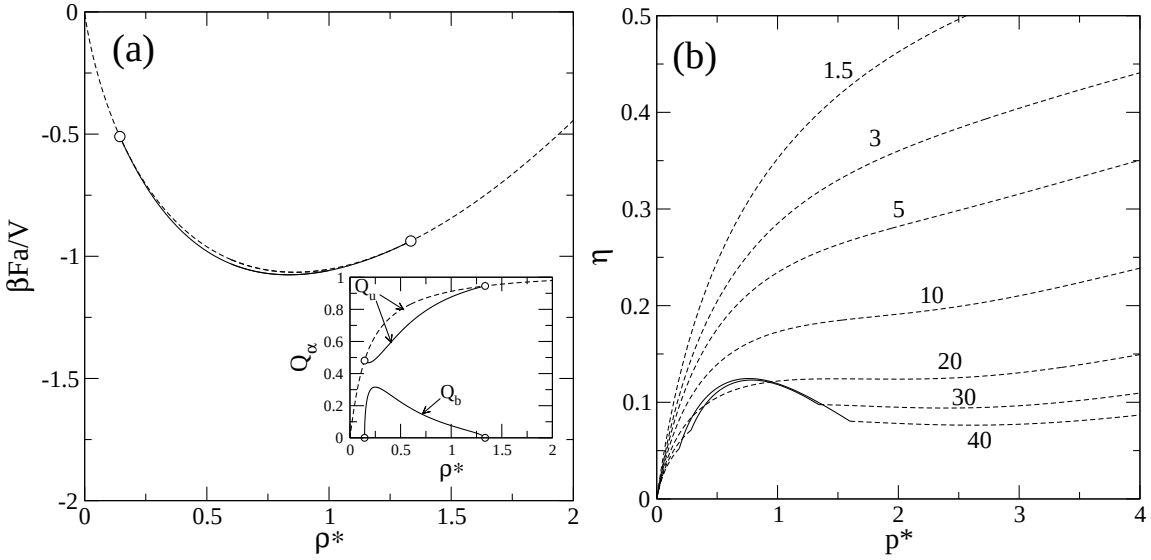

FIG. 4: (a) Free energies of the N_u (dashed curve) and N_b (solid curve) phases as a function of ρ^* for $\kappa = 40$. Inset: Order parameters Q_u and Q_b (correspondingly labelled) as a function of ρ^* for the N_u (dashed curve) and N_b (solid curve) phases. Open circles indicate the bifurcation points. (b) Packing fraction $\eta(Q_u)$ as a function of the reduced pressure $p* = \beta pa$ for different values of κ (as labelled in the figure). The N_u and N_b branches are plotted with dashed and solid curves, respectively.

projection, η_z, can be computed as

$$\eta_{xy}(Q_u) \equiv (\rho_x + \rho_y)\, L\sigma = \frac{2\rho^*}{3}(1 - Q_u), \quad \eta_z(Q_u) \equiv \rho_z \sigma^2 = \frac{\rho^*}{3\kappa}(1 + 2Q_u). \tag{21}$$

For highly elongated particles the total packing fraction can be approximated as $\eta(Q_u) \simeq \eta_{xy}(Q_u)$. In turn this quantity could coincide with η_{2D} for some values of ρ^* (note that Q_u is a function of ρ^* as obtained from the free-energy minimization with respect to the order parameters). When this occurs the N_u-N_b transition takes place. Note that, from (21), the equality $\eta_{xy} = \eta_{2D}$ could be reached for two different values of ρ^*, $\rho^{*(i)}$ $(i = 1, 2)$ with $\rho^{*(1)} < \rho^{*(2)}$ and $Q_u(\rho^{*(1)}) < Q_u(\rho^{*(2)})$ i.e., for two different fluids with different density and orientational order.

We expect the same phase behavior for freely rotating rods. In particular a reentrant N_b phase might be found for high enough aspect ratios and in the range of packing fractions when the inequality $\rho A(Q_u) > \eta_{2D}$ is fulfilled. Here $A(Q_u)$ is the mean particle area obtained by projecting the volume of a particle that forms an angle θ with respect to the layer

normal on the layer perpendicular to the nematic director, and averaging with respect to the equilibrium angular distribution function $h(\theta)$ corresponding to the equilibrium order parameter $Q_{\rm u}$. $A(Q_{\rm u})$ certainly depends on ρ^*, since $Q_{\rm u}$ is a function of ρ^*. In Fig. 4 (b) we plot the packing fraction η as a function of pressure for different values of κ in the range $1.5 \leq \kappa \leq 40$. For $\kappa < 10$ the curves are always concave, while for higher values of κ concavity is lost in some range of pressures (at high enough pressures concavity is recovered). This behavior is a direct consequence of the loop exhibited by the packing fraction $\eta(Q_{\rm u})$ as ρ^* is increased, as explained above. For $\kappa > \kappa_0$ the curves exhibit a clear maximum in the region where the $\rm N_b$ phase is stable (see the solid curves corresponding to $\kappa = 30, 40$). When the rotational symmetry is broken in the xy plane there is a clear gain in surface area per particle, i.e. more particles can be packed with $\rm N_b$ symmetry.

The bifurcation values of packing fraction η and scaled density $\rho_{\rm 2D}\sigma^2$, as obtained from the solution of (13), are plotted in Fig. 5(a) and (b) as a function of κ^{-1}. As mentioned before, no solutions of Eqn. (13) exist when $\kappa < \kappa_0$ since η_z, the packing fraction of hard squares, is of the order of η_{xy} and the gain in excluded volume obtained by orienting the rectangular species along x ($\gamma_x > \gamma_y$) is not enough to compensate the loss in mixing entropy. As can be seen from Fig. 5(b), the behavior of the lower and upper bifurcation curves are different in the Onsager limit $\kappa \to \infty$. Note that, for $\kappa \gg 1$, Eqn. (13) reduces to

$$y\kappa^2 - 2 = e^{2y\kappa+1}. \tag{22}$$

The lower branch can be obtained from (22) by defining the new variable $\theta = y\kappa^2$ and taking the limit $\kappa \to \infty$, which results in the solution $\theta = 2 + e$. Therefore the asymptotic behaviour of the lower branch is $y_{\rm l} \approx \rho_{\rm 2D}^{(l)}\sigma^2 = (2+e)/\kappa^2$. To find the asymptotic behavior of the upper branch we define another variable, $\tau = y\kappa$. Note that $\tau \to \infty$ when $\kappa \to \infty$, so that Eqn. (22) becomes $\tau\kappa = e^{2\tau}$. A fixed point algorithm $\tau_n = \dfrac{1}{2}\ln(\kappa\tau_{\rm n-1})$ with initial guess $\tau_0 = 1/2$ provides

$$\tau_n = \frac{1}{2}\left\{\ln(\kappa/2) + \ln(\ln(\kappa/2)) + \mathcal{O}\left[\frac{\ln(\ln(\kappa/2))}{\ln(\kappa/2)}\right]\right\}, \tag{23}$$

which, for $\kappa \gg 1$, asymptotically gives

$$\tau^* = \lim_{n\to\infty}\tau_n \sim \frac{1}{2}\left\{\ln(\kappa/2) + \ln(\ln(\kappa/2))\right\}. \tag{24}$$

Thus we have $y_{\rm u} \approx \rho_{\rm 2D}^{(u)}\sigma^2 = \tau^*/\kappa \to 0$ when $\kappa \to \infty$. It is interesting to note that $y_{\rm l} \sim (3+e)x^2$ and $y_{\rm u} \sim -\dfrac{x}{2}\ln(2x)$ (we have defined $x = \kappa^{-1}$). Then we obtain $y_{\rm l}'(x) \sim 2(2+e)x$

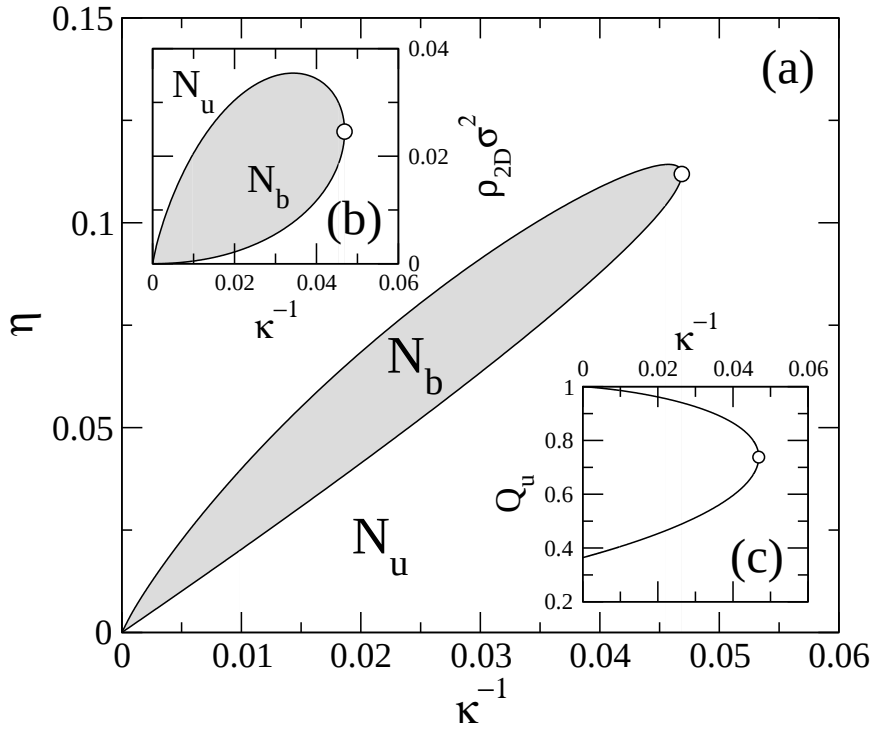

FIG. 5: (a) The N_u-N_b bifurcation values of the packing fraction η as a function of the inverse aspect ratio κ^{-1} found from the solution of Eqn. (13). (b) Bifurcation values for $\rho_{2D}\sigma^2$. (c) Uniaxial order parameter Q_u along the N_u-N_b spinodal.

and $y'_u \sim -\frac{1}{2}\ln(2x)$ for the first derivatives of these functions. Thus we find $y'_l(x) \to 0$ and $y'_u(x) \to \infty$ when $x \to 0$. These limits, together with the limits $y_{l,u}(x) \to 0$, can be checked to hold numerically from Fig. (5)(b) (note that $\rho_{2D}\sigma^2 \sim y$ for $\kappa \gg 1$). Taking into account Eqn. (14) we find that $\eta_l(x) \sim 2x \to 0$ and $\eta_u(x) \sim -\frac{x}{2}\ln(2x) \to 0$, when $x \to 0$, for the lower and upper branches of packing fractions at bifurcation. In the same limit we have $\eta'_l(x) \sim 2$ and $\eta'_u(x) \sim -\frac{1}{2}\ln(2x) \to \infty$, which again can be verified from Fig. 5(a). In the inset (c) we plot the uniaxial order parameter Q_u along the N_u-N_b bifurcation, as obtained from Eqns. (13) and (14). It is interesting to note the relatively low value of the order parameter ($Q_u = 0.36417$) at the point where the N_b solution first bifurcates in the Onsager limit ($\kappa \to \infty$).

We have also performed a bifurcation analysis to study the instability of the nematic against spatially nonuniform fluctuations, such as columnar (C) or crystal (K) fluctuations. We solved Eqns. (11) and (19) to find the values of packing fraction η, order parameter Q_u and wave number $q = 2\pi/d$ (with d the periodicity of the density modulation along a given

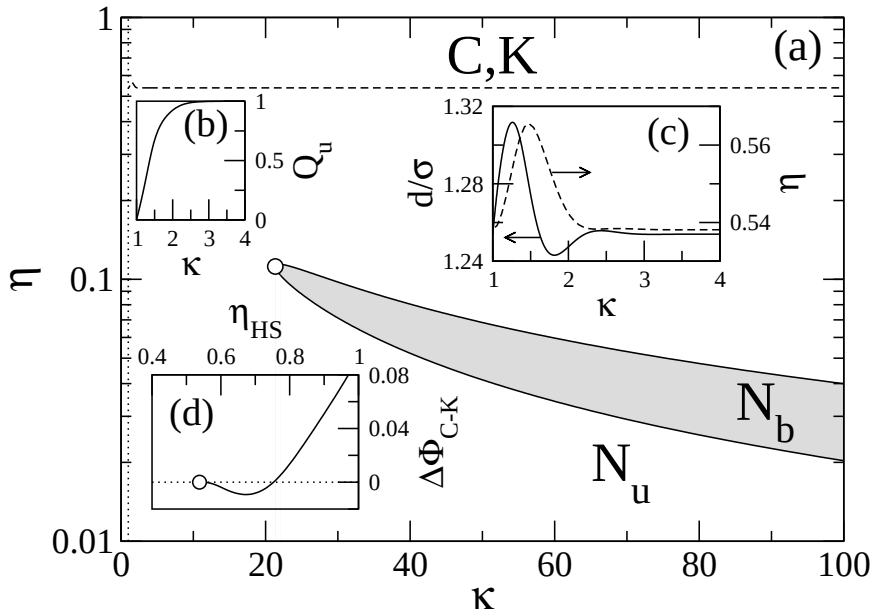

FIG. 6: (a) $\eta - \kappa$ phase diagram of rods in the Zwanzig approximation. The stability region of the N_b phase is shaded in grey and bounded by the solid line. The symbol label the critical end-point. The dashed line represents the N_u-(C,K) spinodal. (b) Uniaxial order parameter Q_u along the latter spinodal. (c) Detail of the N_u-(C,K) packing fraction spinodal (dashed curve) and period in reduced units of the nonuniform phases at bifurcation (solid curve). (d) The free-energy difference between the C and K phases ($\Phi \equiv \beta \mathcal{F} a/V$, $\Delta\Phi_{C-K} = \Phi_C - \Phi_K$) as a function of the two-dimensional packing fraction, $\eta_{HS} = \rho_{HS}\sigma^2$, for a one-component fluid of hard squares of sizes σ.

direction) at bifurcation. The results are plotted in Figs. 6(b) and (c) for $1 \leq \kappa \leq 4$. As can be seen, the spinodal values of the packing fraction do not change too much as κ is varied [see dashed line in panel (c)]. The same behaviour occurs with the period in reduced units d/σ as a function of κ [solid line in panel (c)]. This periodicity corresponds to that of the C or K phases with a high proportion of hard squares [see the evolution of the order parameter Q_u along the spinodal in panel (b)]. For larger values of κ, as $Q_u \to 1$, the packing fraction tends asymptotically to that of the N-(C,K) bifurcation of the one-component fluid of hard squares, i.e. $\kappa = 1$ (note that the C and K phases bifurcate at the same point).

All of the above results, i.e. those for the N_u-N_b continuous transition (Fig. 5), and those from the bifurcation analysis to nonuniform phases, are collected in Fig. 6(a), which is the complete phase diagram in the $\eta - \kappa$ plane. The only remaining question is the relative stability of the C and K phases at high densities. For the one-component fluid of hard

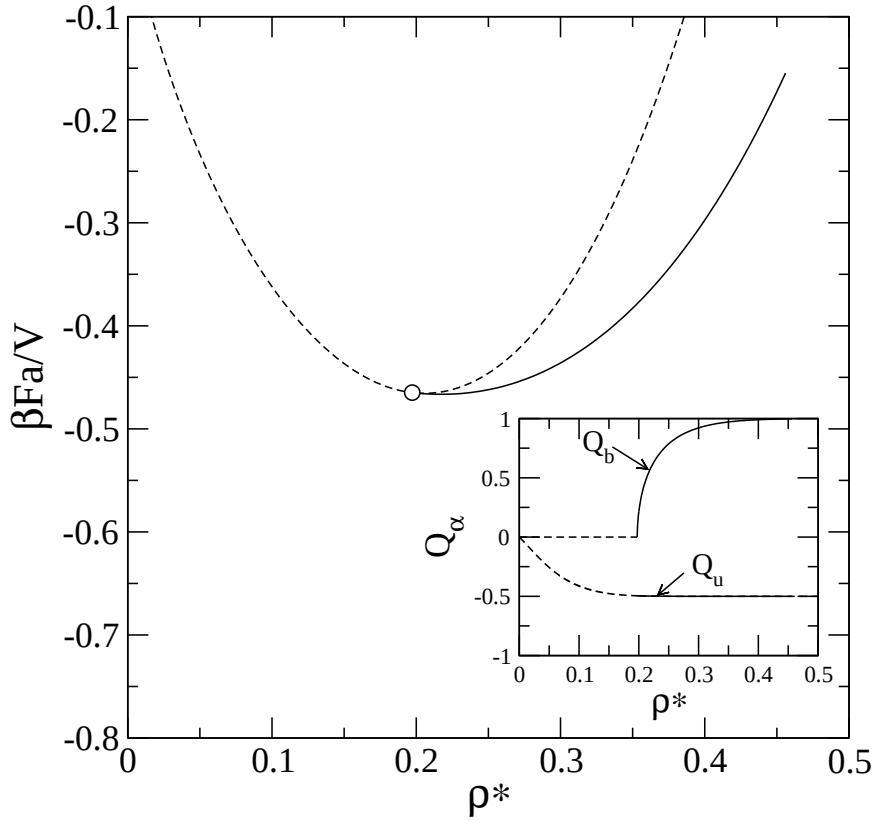

FIG. 7: Free energies of N_u (dashed curve) and N_b (solid curve) phases as a function of ρ^* for $\kappa^{-1} = 10$. The open circle indicates the bifurcation point. Inset: The evolution of the order parameters Q_u and Q_b as a function of ρ^* along the N_u (dashed curve) and N_b (solid curve) branches.

squares, both phases bifurcate at $\eta_{HS} \equiv \rho_{HS}\sigma^2 = 0.5381$. The C is more up to $\eta_{HS} \sim 0.75$, beyond which the K phase becomes stable up close packing [see Fig. 6(c)]. In our system (a ternary mixture of hard squares and mutually orthogonal hard rectangles) and for high enough κ (in particular for $\kappa > 4$), we expect the same phase behaviour due to the small fraction of rectangular species at densities close to the spinodal instabilities (when $Q_u \sim 1$). For $1 \leq \kappa \leq 4$ a free-energy minimization of the ternary mixture in needed to elucidate this question. However we expect that the C phase will be the most stable phase, due to the fact that it is difficult to pack a ternary mixture of anisotropic species within a regular crystalline lattice.

B. Oblate particles

The phase behavior of oblate particles is characterized by a much wider region of stability of the N_b phase. This in turn can be explained by resorting to Figs. 2(c) and (d). Now the projection of the parallelepipedic species z (now $\sigma > L$ and consequently $\kappa < 1$) form squares with surface area σ^2. The other two species, x and y, are rectangles with mutually orthogonal orientations of side-lengths σ and L, with particle areas ($L\sigma$) much lower than that of the z-species, in particular when κ is small enough. Therefore, as density is increased, the averaged excluded volume is lowered when the main particle axis lies in the xy plane, and the uniaxial order parameter Q_u decreases from zero and tends asymptotically to -0.5 for high enough densities. Furthermore, since the system is quasi-two-dimensional, it exhibits a N_u-N_b continuous phase transition at packing fractions $\sim \eta_{2D}$ (the packing fraction of the strictly two-dimensional fluid of hard rectangles).

This behavior is shown in Fig. 7, where the free-energy branches of the N_u and N_b phases are plotted as a function of ρ^*. The inset shows the evolution of the order parameters Q_u and Q_b as a function of the same variable. Q_b departs from zero at the N_u-N_b bifurcation point. Beyond this point the N_b is the most stable phase up to densities corresponding to the instabilities of the N_b phase against spatially nonuniform fluctuations. These densities are calculated via the bifurcation analysis of Sec. II B, and are plotted in the phase diagram of Fig. 8(a). Note the strong oscillations exhibited by the spinodal curve when $1 \leq \kappa^{-1} \leq 4$ [i.e. the interval in which the biaxial order parameter Q_b is zero, see panel (c)]. This is because of the vanishingly small fraction of squares, with the rectangular species being parallel to the x or y axes with equal probability. Thus, when the particle anisotropy grows, it becomes more difficult to commensurate the characteristic lengths of both rectangular species within the single lattice parameter of a nonuniform phase [C, K or smectic (S)]. The oscillations could have different origins: (i) when the ratio between the long and short edges of the rectangles is close to an integer number, square clusters can be formed by joining the rectangles along their long sides. These clusters in turn can be accommodated into an square crystalline superlattice. (ii) The transitions to nonuniform phases could change from continuous to first order, with the coexisting density corresponding to the N_u phase located well below that estimated from the bifurcation analysis. (iii) The relative stability of C, S and K phases could strongly change with κ. In Fig. 8(b) the uniaxial order parameter Q_u

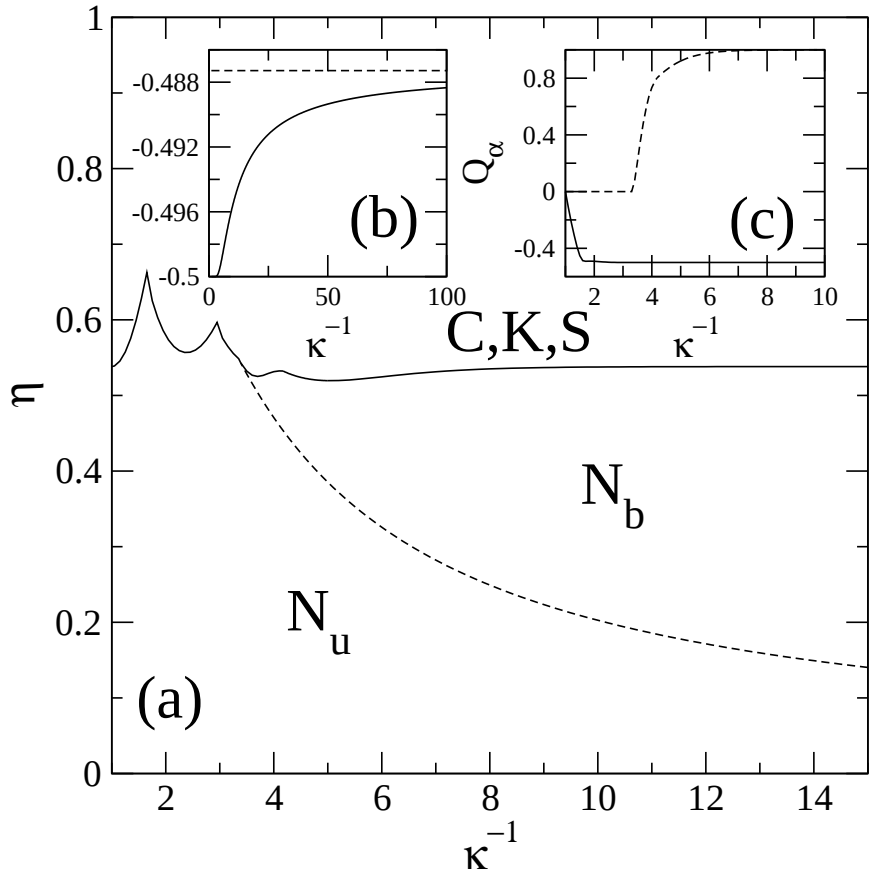

FIG. 8: (a) $\eta - \kappa$ phase diagram of rods in the Zwanzig approximation. The dashed line represents the location of the continuous N_u-N_b transition, while the spinodal curve for the $N_{u,b}$ instability against non-uniform (C, K or S) phases is shown with solid line. (b) Uniaxial order parameter Q_u along the N_u-N_b transition (solid curve) and its asymptotic value for $\kappa \to 0$ (dashed curve). (c) Uniaxial (solid curve) and biaxial (dashed curve) order parameters along the spinodal curve corresponding to nonuniform phase instabilities.

along the N_u-N_b bifurcation is plotted. It is important to note that, in the asymptotic limit $\kappa \to 0$, we have $Q_u \to -0.4873$, i.e. biaxial ordering appears in particle configurations with a residual proportion of hard squares.

Finally, in Fig. 9(a) we plot $\Delta\rho^*$, i.e. the difference between the spinodal curves corresponding to the three-dimensional Zwanzig oblate particles with their centers of mass located on a plane and the strictly two-dimensional system of Zwanzig hard rectangles. As we can see, the N_u-N_b transition curve practically coincides with that of the I-N_u in 2D. The difference between the spinodal curves corresponding to transitions to nonuniform phases

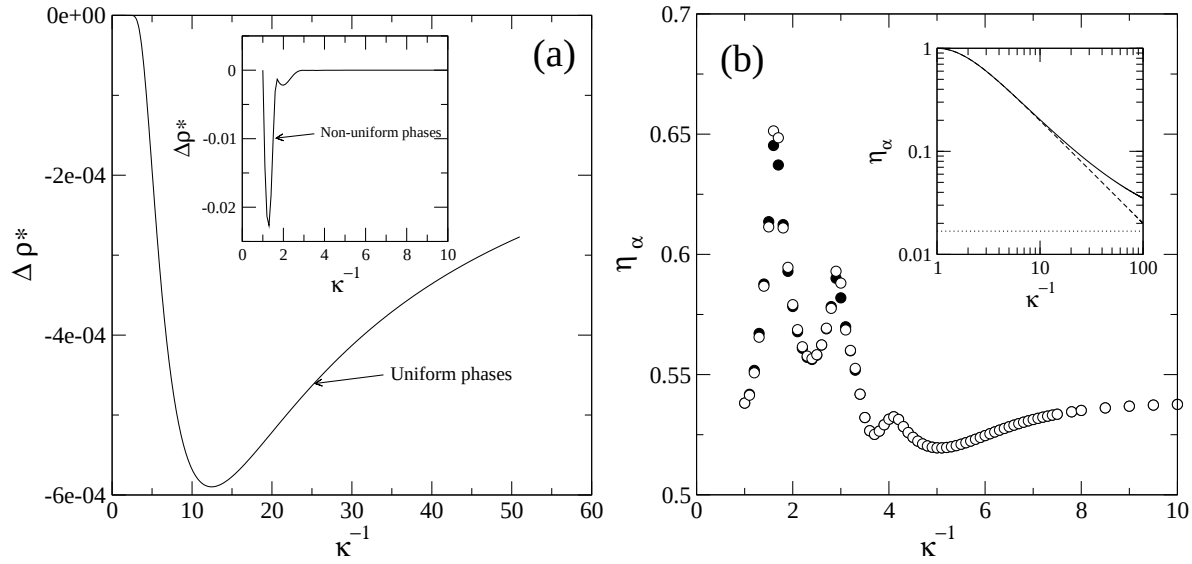

FIG. 9: (a) Difference $\Delta\rho^*$ between the transition and spinodal curves of confined plates. Main figure: Difference between the density of the N_u-N_b transition in 3D and that of the I-N_u transition in 2D. Inset: Difference between the $N_{u,b}$-(C,K,S) spinodals in 3D and (I,N_u)-(C,K,S) spinodals in 2D. (b) Packing fractions η corresponding to the instability with respect to nonuniform phases for the monolayer of plate-like particles (empty circles) and for a strictly two-dimensional model (solid circles). Inset: The packing fractions corresponding to the N_u-N_b (solid) and I-N_u (dashed) transitions for the monolayer and the two-dimensional model, respectively. The asymptotic packing fraction η_a (see the text) is shown with dotted line.

is larger for $1 < \kappa^{-1} < 2$, i.e., in the region where the strong oscillations in the spinodal take place. In the main figure of Fig. 9(b) we plot, for comparison, the nonuniform phase spinodals corresponding to the plates monolayer (empty circles) and to the two-dimensional hard rectangles (solid circles). The conclusion is that they are practically the same. The inset in panel (b) shows the N_u-N_b spinodals for both systems. The main difference is related to the asymptotic limit $\kappa \to 0$. For the two-dimensional system, the usual Onsager result $\eta \to 0$ results, while for the monolayer of plates the system retains a residual packing fraction $\eta_a = 0.01681$, a result directly connected with the non-perfect uniaxial ordering ($Q_u \neq -0.5$) of plates, as already discussed above.

IV. CONCLUSIONS

Taking advantage of the $3D \to 2D$ dimensional crossover property of the fundamental measure density functional for the Zwanzig model, we have studied the phase behaviour of a monolayer of rod-like or plate-like uniaxial particles. We have focused, in particular, on their orientational ordering properties. Despite the fact that particles are uniaxial (they have only two characteristic lengths L and σ), we have shown the presence of a N_u-N_b phase transitions for both particle geometries. For rod-like geometry, the N_b is a reentrant phase, since its region of stability in the phase diagram (aspect ratio-density plane) is always surrounded by that of the N_u phase. For this geometry the N_u-N_b transition is continuous and the two N_u-N_b transitions bounding the region of N_b stability meet at the critical end-point (κ_0, ρ_0^*). For $\kappa < \kappa_0$ only the N_u is stable. For particles with large aspect ratio, there is inversion in the packing fraction with respect to the uniaxial order parameter. For plate-like geometry, there exists a single continuous transition line separating the regions of N_u and N_b phase stabilities. This line crosses the spinodal instability to nonuniform phases at higher densities. The crossing point is approximately located at $\kappa \approx 0.3$. Therefore, below this aspect ratio, the N_b is stable at high enough densities until a point where stability with respect to C, S or K phases is lost. Above this aspect ratio the N_u is the only stable orientationaly-ordered phase; at higher densities it again looses stability with respect to nonuniform phases. We have shown that the phase diagram of monolayers of plate-like particles is very similar to that of the strictly two-dimensional hard rectangular fluid in the restricted-orientation approximation.

At present MC simulations of freely-rotating hard oblate ellipsoids with centers of mass confined on a plane are being carried out [26]. We expect to find a qualitative agreement between the results obtained from the present model and the simulations.

Acknowledgments

We gratefully acknowledge illuminating discussions with G. Odriozola. Financial support from Comunidad Autónoma de Madrid (Spain) under the R&D Programme of Activities MODELICO-CM/S2009ESP-1691, and from MINECO (Spain) under grants FIS2010-22047-C01 and FIS2010-22047-C04 is acknowledged. SV acknowledges the financial support of the

Hungarian State and the European Union under the TAMOP-4.2.2.A-11/1/KONV-2012-0071.

[1] A.B.G.M. Leferink op Reinink, E. van den Pol, A.V. Petukhov, G.J. Vroege and H.N.W. Lekkerkerker, Eur. Phys. J. **222**, 3053 (2013).

[2] P. J. Camp, C. P. Mason, M. P. Allen, A. A. Khare and D. A. Kofke, J. Chem. Phys. **105**, 2837 (1996).

[3] J. A. Cuesta and D. Frenkel, Phys. Rev. A **42**, 2126 (1990).

[4] D. Frenkel and R. Eppenga, Phys. Rev. A **31**, 1776 (1985).

[5] M. D. Khandkar and M. Barma, Phys. Rev. E **72**, 051717 (2005).

[6] U. Tkalec and I. Muševič, Soft Matter **9**, 8140 (2013).

[7] Wen-Sheng Xu, Yan-Wei Li, Zhao-Yan Sun, and Li-Jia An, J. Chem. Phys. **139**, 024501 (2013).

[8] M. E. Foulaadvand and M. Yarifard, Phys. Rev. E **88**, 052504 (2013).

[9] Z. Zheng, F. Wang and Y. Han, Phys. Rev. Lett. **107**, 065702 (2011).

[10] C. K. Mishra, A. Rangarajan and R. Ganapathy, Phys. Rev. Lett. **110**, 188301 (2013).

[11] Y. Han, A. Alsayed, M. Nobili and A. G. Yodh, Phys. Rev. E **80**, 011403 (2009).

[12] N. F. Bouxsein, C. Leal, C. S. McAllister, K. K. Ewert, Y. Li, C. E. Samuel and C. R. Safinya, J. Am. Chem. Soc. **133**, 7585 (2011).

[13] T. E. Herod and R. S. Duran, Langmuir **14**, 6606 (1998).

[14] H. Razafindralambo, A. Richel, M. Paquot, L. Lins and C. Blecker, J. Phys. Chem. B **116**, 3998 (2012).

[15] X. Ye, J. Chen, M. Enger, J. A. Milan, W. Li, L. Qi, G. Xing, J. E. Collins, C. R. Kagan, J. Li, S. C. Glotzer and C. B. Murray, Nature Chemistry **5**, 466 (2013).

[16] M. A. Bates and D. Frenkel, J. Chem. Phys. **112**, 10034 (2000).

[17] Y. Martínez-Raton, E. Velasco, and L. Mederos, J. Chem. Phys. **122**, 064903 (2005).

[18] A. M. Somoza and R. C. Desai, J. Phys. Chem. **96**, 1401 (1992).

[19] D. Kramer, A. Ben-Shaul, Z.-Y. Chen and W. M. Gelbart, J. Chem. Phys. **96**, 2236 (1992).

[20] F. Kim, S. Kwan, J. Akana, and P. D. Yang, J. Am. Chem. Soc. **123**, 4360 (2001).

[21] E. Van den Pol, A. V. Petukhov, D. M. E. Byelov and G. J. Vroege, Phys. Rev. Lett. **103**, 258301 (2009).

[22] Y. Martínez-Ratón, S. Varga and E. Velasco, PCCP **13**, 13247 (2011).

[23] S. Belli, A. Patti, M. Dijkstra and R. Van Roij, Phys. Rev. Lett. **107**, 148303 (2011).

[24] S. D. Peroukidis and A. G. Vanakaras Soft Matter **9**, 7419 (2013).

[25] J. A. Cuesta and Y. Martínez-Ratón, Phys. Rev. Lett. **78**, 3681 (1997).

[26] G. Odriozola, Private comunication.